Electron-impact ionization cross section of rubidium

Yong-Ki Kim
National Institute of Standards and Technology, Gaithersburg, Maryland 20899

Jacek Migdałek and Wojciech Siegel
Institute of Physics and Computer Science, Cracow Pedagogical University, 30-084 Kraków, Poland

Jacek Bieroń
Institute of Physics, Jagellonian University, 30-059 Kraków, Poland

(Received 12 June 1997)

A theoretical model for electron-impact ionization cross section has been applied to Rb and the theoretical cross section (from the threshold to 1 keV in incident energy) is in good agreement with the recent experimental data obtained using Rb atoms trapped in a magneto-optical trap. The theoretical model, called the binary-encounter–dipole (BED) model, combines a modified Mott cross section with the high-energy behavior of Born cross sections. To obtain the continuum dipole oscillator strength df/dE of the $5s$ electron required in the BED model, we used Dirac-Fock continuum wave functions with a core polarization potential that reproduced the known position of the Cooper minimum in the photoionization cross section. For inner-shell ionization, we used a simpler version of df/dE, which retained the hydrogenic shape. The contributions of the $4p \rightarrow 4d$, $5s$, and $5p$ autoionizing excitations were estimated using the plane-wave Born approximation. As a by-product, we also present the dipole oscillator strengths for the $5s \rightarrow np_{1/2}$ and $5s \rightarrow np_{3/2}$ transitions for high principal quantum numbers n near the ionization threshold obtained from the Dirac-Fock wave functions with the same core polarization potential as that used for the continuum wave functions. [S1050-2947(98)02601-8]

PACS number(s): 34.80.Dp

I. INTRODUCTION

Owing to their simple electronic structure, alkali-metal atoms have served as a favorite testing ground for theoretical models that simplify the task of describing atomic properties such as electron correlation and their interaction with photons [1–4]. The most popular procedure is to introduce a model potential to represent the interaction between the lone valence electron and the core in lieu of the core-valence electron correlation and then calculate properties such as the f values for discrete transitions and photoionization cross sections.

In addition, the fact that the ratio between the f value for the $ns \rightarrow n'p_{3/2}$ transition and that for the $ns \rightarrow n'p_{1/2}$ for $n' > n$ for Rb and Cs departs markedly from the 2:1 ratio predicted by the LS coupling has attracted the attention of both experimental and theoretical investigators from the early days of quantum mechanics [5,6].

The electron-impact ionization cross section of Rb has been measured since the 1930s [7–10], but only very simple theoretical models had been available [11–13] for comparison. The existing theoretical models predicted only the direct ionization of the bound electrons, while the experiments included contributions from the autoionizing excitations of the $4p$ electrons to the $4d$, $5s$, and $5p$ states. As will be shown later, these autoionizing excitations contribute almost one-third of the total ionization cross section near the peak at the incident energy $T \sim 35$ eV.

Very recently, Schappe *et al.* [14] bombarded Rb atoms trapped in a magneto-optical trap with electrons and obtained an absolute total ionization cross section. This experiment actually measured the number of ionizing events, known as the counting ionization cross section, in contrast to the ion-current measurements, known as the gross ionization cross section, carried out in the past. Usually, theory predicts a counting ionization cross section, which is smaller than the corresponding gross ionization cross section by definition:

$$\sigma_{gross} = \Sigma_k k \sigma^{k+}, \tag{1}$$

while

$$\sigma_{counting} = \Sigma_k \sigma^{k+}, \tag{2}$$

where k denotes the charge state and σ^{k+} denotes the cross section for producing a Rb^{k+} ion.

Unlike some old measurements, however, the recent experiment by Schappe *et al.* covered incident energies $T \geqslant 50$ eV, which is beyond the two leading peaks in the ionization cross section: the first one at $T \sim 12$ eV from the ionization of the $5s$ electron and the second one at $T \sim 35$ eV from the autoionizing excitations of the $4p$ electrons mentioned earlier. Kim and Rudd [15] developed a theoretical model for electron-impact ionization called the binary-encounter–dipole (BED) model. The BED cross sections for light atoms, such as H, He, and Ne, were found to agree very well with known experiments from ionization thresholds to a few keV in T when the continuum dipole oscillator strengths df/dE, where E is the photon energy, were known.

The application of the BED model to Rb poses two major challenges. The first challenge is to see whether the BED model can be applied to an atom much larger than Ne. Actually, a simpler version of the BED model was found to be very effective in reproducing the known total ionization cross sections of molecules [16–18], ranging from H_2 to SF_6

and neutral molecules and radicals alike, from ionization thresholds to a few keV in T, very much like our experience with the light atoms. The simpler version, called the binary-encounter–Bethe (BEB) model, replaces df/dE with a much simpler function that mimics the shape of hydrogenic df/dE. We used the BEB model for inner-shell ionization, whose contribution is small, while using the BED model for the ionization of the $5s$ electron, which dominates the total ionization cross section.

The second challenge is that we still have to find accurate df/dE for the ionization of the $5s$ electron. To apply the BED model, we need df/dE for photon energies from the ionization threshold to a few hundred eV. However, the most reliable experimental data on the photoionization of Rb [19] covered only low photon energies and the data were normalized to an earlier theory by Weisheit [1], who used a model potential to calculate the photoionization cross section. The main focus of this experiment was to identify the position of a minimum, known as the Cooper minimum, in the photoionization cross section approximately 0.8 eV above the threshold. In other words, the experimental cross section is likely to have reproduced the shape of the photoionization cross section near the Cooper minimum very well, but the absolute magnitude should be reexamined in view of other theoretical and experimental evidence.

The df/dE, or the photoionization cross section, of the $5s$ electron is unusually small not only because of the Cooper minimum near the threshold, where the cross section should have been substantial otherwise, but also because most of the oscillator strengths lie in the $5s\rightarrow np$ discrete excitations. For instance, the sum of the f values for the $5s\rightarrow 5p_{1/2}$ and $5s\rightarrow 5p_{3/2}$ transitions is already 1.06 according to our estimate presented below.

To deduce a reliable df/dE that is also compatible with the known f values for the discrete excitations, we used a modified form of the core polarization potential method proposed by Migdałek and Baylis [3] to generate Dirac-Fock wave functions for the discrete and continuum wave functions and calculated matching discrete f values and df/dE. The cutoff radius required in the modified dipole transition operator was chosen so that the position of the theoretical Cooper minimum in the df/dE coincides with that observed in the experiment by Suemitsu and Samson [19].

To estimate the contributions from the numerous $4p\rightarrow 4d$, $5s$, and $5p$ autoionizing excitations, we used the Dirac-Fock wave functions generated without any core polarization potential with the plane-wave Born approximation. Since the core polarization potential represents the effect of valence-core correlation on the valence electron, it is inappropriate to use the potential for the excitation of the $4p$ electrons.

The BED and BEB models and the core polarization potential method are briefly described in Sec. II. The resulting f values for discrete excitations and the df/dE of the $5s$ electron are presented and compared with existing theoretical and experimental results in Sec. III, while our electron-impact ionization cross section is compared with the available experimental data in Sec. IV. Conclusions are presented in Sec. V.

II. THEORY

As mentioned in Sec. I, we used the theoretical model developed by Kim and Rudd [15] for the direct ionization of all bound electrons by electron impact and the plane-wave Born approximation for the electron-impact excitation of the $4p$ electrons to the numerous levels associated with the $4p^5 5s^2$, $4p^5 5s 4d$, $4p^5 5s 5p$, $4s 4p^6 5s^2$, and $4s 4p^6 5s 5p$ configurations. To calculate df/dE for the ionization of the $5s$ electron, we used a modified form of the core polarization potential (CPP) model developed by Migdałek and Baylis [3] to generate the ground-state and continuum wave functions using the Dirac-Fock wave-function code originally written by Desclaux [20]. The continuum wave-function code uses frozen-core orbitals ($1s^2 2s^2$, . . . ,$4s^2 4p^6$) to solve for self-consistent $\epsilon p_{1/2}$ and $\epsilon p_{3/2}$ continuum orbitals, where ϵ is the photoelectron energy, with full exchange interaction with the core orbitals. The CPP was included in the Dirac-Fock equations only for the valence electron to generate all discrete and continuum wave functions. In addition, the dipole transition operator was also modified in accordance with the CPP model as explained below.

A. Binary-encounter–dipole model

The BED model developed by Kim and Rudd [15] combines a modified form of the Mott cross section [21,22] and the high-incident-energy behavior of the Bethe theory [23,24]. Unlike many previous attempts to combine these two theories, the BED model begins with the singly differential ionization cross section $d\sigma/dW$, where W is the ejected electron energy, and requires both the integrated (total) ionization cross section

$$\sigma_i = \int (d\sigma/dW) dW \tag{3}$$

and the stopping cross section

$$\sigma_{stop} = \int (W+B)(d\sigma/dW) dW, \tag{4}$$

where B is the binding energy of the ejected electron, to match the appropriate high-T form predicted by the Bethe theory. The stopping cross section is used in evaluating the stopping power [24].

The Bethe theory for ionization predicts the dominance of dipole interaction in electron-impact ionization at large values of T/B and hence the continuum dipole oscillator strength df/dE enters in the formulation of the BED model. In electron-impact ionization, E plays the role of energy loss of the incident electron, i.e., $E=W+B$. Hence we shall use df/dE interchangeably with df/dW because B is a constant for a given orbital.

The BED model predicts both the differential and total ionization cross sections for the direct ionization of bound electrons in each atomic orbital and hence the df/dE required in the BED model is for the photoionization of electrons in each atomic orbital. In principle, df/dE can be deduced from experimental photoionization cross sections if orbital-by-orbital partial cross sections are known. However, most experimental photoionization cross sections are total

cross sections, from which differential cross sections may not be extracted easily. Moreover, df/dE from the ionization threshold to several hundred eV above the threshold in photon energy is needed to integrate the differential cross section and obtain a reliable total ionization cross section. The procedure we have used to calculate df/dE is described in Sec. III.

According to the BED model, σ_i of an atomic orbital with the binding energy B, the average kinetic energy $U=\langle \boldsymbol{p}^2/2m \rangle$, $\boldsymbol{p}$ and m being the momentum and the electron mass, respectively, and the electron occupation number N is obtained by integrating $d\sigma/dW$ over the allowed range of W, i.e., from 0 to $(T-B)/2$:

$$\sigma_{BED}(t)=\frac{S}{t+u+1}\left[D(t)\ln t+\left(2-\frac{N_i}{N}\right)\left(\frac{t-1}{t}-\frac{\ln t}{t+1}\right)\right], \tag{5}$$

where $t=T/B$, $u=U/B$, $S=4\pi a_0^2 N R^2/B^2$, $a_0=0.5292$ Å, $R=13.61$ eV,

$$D(t)\equiv N^{-1}\int_0^{(t-1)/2}\frac{1}{w+1}\frac{df(w)}{dw}dw, \tag{6}$$

with $w=W/B$, and

$$N_i\equiv\int_0^{\infty}\frac{df(w)}{dw}dw. \tag{7}$$

Equations (6) and (7) involve integration of df/dw and hence we fitted the calculated df/dw with power series in inverse powers of w to facilitate the integration to arbitrary t as is shown in Sec. III.

On the right-hand side of Eq. (5), the first logarithmic term represents the dipole interaction predicted by the Bethe theory and the last logarithmic term arises from the interference between the direct and exchange interactions described by the Mott cross section. The $(t-1)/t$ term arises from close collisions with large momentum transfers between the incident and ejected electrons. We used Eq. (5) to calculate the ionization cross section of the $5s$ electron.

B. Binary-encounter–Bethe model

Equation (5) requires explicit knowledge of df/dw for each orbital. Although such df/dw can be calculated for atoms at the same level of approximation we have used for the $5s$ orbital, a simpler approximation, the BEB model, was found to be sufficient when only a modest accuracy ($\sim 10\%$) was required [15–17]. The BEB model uses an approximation to df/dw [15], i.e.,

$$df/dw=N/(w+1)^2, \tag{8}$$

such that the integrated cross section σ_i with Eq. (8) is given by [15]

$$\sigma_{BEB}(t)=\frac{S}{t+u+1}\left[\frac{\ln t}{2}\left(1-\frac{1}{t^2}\right)+1-\frac{1}{t}-\frac{\ln t}{t+1}\right]. \tag{9}$$

The shape of df/dw given by Eq. (8) resembles the shape of the df/dw for the photoionization of the $1s$ electron in the hydrogen atom. We used Eq. (9) for the ionization of all core orbitals, though the contributions from the K and L shells are negligible and can be omitted for $T\leqslant 1$ keV. We used experimental binding energy for the $5s$ electron to ensure proper threshold for ionization, while we used $2j+1$ weighted average values of theoretical B and U for other orbitals. Orbital energies were used in lieu of the binding energies according to the Koopmans theorem. The values of B, U, and N for Rb are listed in Table I.

TABLE I. Atomic orbital, electron binding energy B in eV, kinetic energy U in eV, and electron occupation number N for Rb. All values are theoretical, except that the binding energy of the $5s$ orbital is experimental. Orbital energies are used as the binding energies. Dirac-Fock values of B and U were averaged with $2j+1$ weight, for instance, $B(3d)=[4B(3d_{3/2})+6B(3d_{5/3})]/10$. The U values marked, e.g., 938.76/3, denote the kinetic-energy value divided by the principal quantum number U/n as explained in Sec. II B.

Orbital	B	U/n	N
$3s$	341.77	938.76/3	2
$3p$	260.71	856.79/3	6
$3d$	126.63	713.17/3	10
$4s$	42.62	146.82/4	2
$4p$	21.99	108.47/4	6
$5s$	4.18	8.81/5	1

In the binary-encounter theory, the $u+1$ term in the denominator of Eqs. (5) and (9) has been introduced based on the argument that the effective potential-energy difference between the incident and bound electrons is not T but $T+U+B$. However, the U value of an orbital with many radial nodes is rather high compared to B and we found that U/n, where n is the principal quantum number of the orbital, rather than U itself produced much better agreement with experiment in many applications [16,17]. Hence we used U/n in the BEB and BED cross sections of the electrons in the M and N shells as well as the $5s$ electron.

C. Core-polarization-potential method

One of the drawbacks of most atomic collision theories is neglect of electron correlation between the valence electrons being excited or ionized and those of the ion core. This part of correlation effects (called core-valence electron correlation) can conveniently be represented by a classical model as polarization of the core by the valence electron (a concept used in quantum-mechanical calculations by Biermann [25], although the origin of the core-polarization picture can be traced back even to the semiclassical study of the helium atom by Heisenberg [26] in 1926).

The most complete quantum approach to the core-polarization effect was presented by Böttcher and Dalgarno [27]. Their theory, which is based on a perturbation approach, leads to asymptotic forms of core polarization potential V_p and corrected dipole transition moment $\boldsymbol{d}_{eff}$, which are in agreement with the classical formulas.

We emphasize here that neither classical nor quantum-mechanical approaches provide the form of the core-polarization corrections for the small- or intermediate-r re-

gion. Moreover, the asymptotic form for large r diverges for $r \to 0$. Therefore, there is a need to introduce an arbitrary cutoff function to remove this divergence at $r=0$.

Migdałek and Baylis [28] proposed introducing a cutoff function directly into the expression for the effective field $\boldsymbol{E}_v$ produced by a valence electron at the core and subsequently obtained the following expressions for V_p and $\boldsymbol{d}_{eff}$:

$$V_p = -\frac{\alpha_d r^2}{2(r^2+r_c^2)^3}, \tag{10}$$

$$\boldsymbol{d}_{eff} = -\boldsymbol{r}\left[1-\frac{\alpha_d}{(r^2+r_c^2)^{3/2}}\right], \tag{11}$$

where α_d is the static dipole polarizability of the core and r_c is the cutoff radius.

The core-polarization potential V_p [Eq. (10)] and the matching form of the dipole transition operator [Eq. (11)] were introduced into a Dirac-Fock wave function code [28] and used successfully in numerous applications. In the present study we also adopted these formulas in a modern version of the Dirac-Fock wave function code to account for the core-polarization effect in discrete and continuum dipole oscillator strengths.

III. DISCRETE AND CONTINUUM DIPOLE OSCILLATOR STRENGTHS

The core-polarization corrections presented in the preceeding section require the static dipole polarizability of the core α_d and the cutoff radius r_c. Usually, the static dipole polarizability is calculated separately for the ion. For Rb we adopted the value of $9.076a_0^3$ calculated by Johnson *et al.* [29] for Rb^+ with the relativistic random-phase approximation. It is also common to use the same value of the cutoff radius r_c in both Eqs. (10) and (11) and is most often set to the mean radius of the outermost orbital of the unpolarized core. Although past experience demonstrated that such a choice was satisfactory for the resonance and low-lying discrete transitions [4], we found that it was necessary to modify this practice for *ab initio* calculations of high Rydberg transitions and particularly for continuum transitions. In the present work the cutoff radius in the core-polarization potential [Eq. (10)] was, as usual, set to the mean radius of the outermost orbital of the unpolarized core ($r_c^p = 1.7305a_0$), while the cutoff radii in the dipole transition operator were chosen to reproduce the experimentally known position of the Cooper minimum [19] separately for the $p_{1/2}$ and $p_{3/2}$ fine-structure components ($r_c^d = 1.1 \times r_c^p = 1.9035a_0$ for $p_{1/2}$ and $r_c^d = 1.2 \times r_c^p = 2.0765a_0$ for $p_{3/2}$).

The Dirac-Fock (DF) calculations are most accurate if performed in the relaxed core approximation, i.e., allowing for complete relaxation of all orbitals for each level. However, our continuum wave-function code requires a frozen core and relaxes only the valence orbital in the continuum. For high Rydberg states, we have confirmed that the f values for the $5s \to np$ transitions for high n with fully relaxed initial and final states approach the f values calculated using the frozen core of the Rb^+ ion for the excited states, as expected. Hence we used the same Rb^+ frozen core to calculate the wave functions for all Rydberg states and the continuum.

A. Discrete dipole oscillator strengths

Table II presents the f values calculated in the present study for the principal series in Rb as well as the f-value ratios for the fine-structure components and compares them to available theoretical and experimental data. In addition to the oscillator strengths calculated with the cutoff radii (in dipole transition moments) adjusted to reproduce the experimental Cooper minimum in the continuum (DF+CPII calculations), we have included two other sets of f values. The first set (DF+CPI) was obtained using the same value of the cutoff radius (set to the mean radius of the outermost orbital of the unpolarized core) in both core-polarization potential and induced dipole transition operator. In the second set (labeled DF), the core-polarization corrections were entirely omitted. All computations have been performed using the frozen Rb^+ ion core for the $np_{1/2}$ and $np_{3/2}$ states as described in Sec. II.

The experimental results quoted in Table II have been measured in absorption by Caliebe and Niemax [30], while Shabanova and Khluystalov [31] used the hook method.

Recently, (see [32]) Niemax remeasured oscillator strength ratios by a laser absorption technique, but was not able to confirm his previous results for $n \geq 14$. Therefore, we recalculated his earlier f values for the weaker $5s \to np_{1/2}$ transitions for $n \geq 13$ employing his more recent ratios and his earlier data for the stronger $5s \to np_{3/2}$ transitions, which we found to be more reliable and in good agreement with the data by Shabanova and Khlyustalov. As can be seen from all sets of experimental data, substantial deviations can be observed in the f-value ratios $\rho = f(5s \to np_{3/2})/f(5s \to np_{1/2})$ from the statistical ratio of 2.

This deviation was studied by Fermi [6] and was attributed to the spin-orbit interaction, which in the relativistic picture results in different radial transition integrals for the $np_{1/2}$ and $np_{3/2}$ levels. Actually, there are three factors responsible for the large deviation in the oscillator strength ratio: spin-orbit interaction, cancellation of dipole transition integrals, and core polarization. This deviation sharply increases for the principal series with increasing principal quantum number n of the upper level. The spin-orbit interaction distinguishes $np_{1/2}$ and $np_{3/2}$ radial wave functions, though the spin-orbit interaction diminishes as n^{-3}. The core polarization amplifies the difference between the $np_{1/2}$ and $np_{3/2}$ orbitals because the CPP affects the two orbitals differently. Finally, the cancellation of the radial transition integrals, which eventually produces the Cooper minimum, further enhances the departure of ρ from the statistical value [33].

The $np_{1/2}$ orbitals are more seriously affected by correlation than the $np_{3/2}$ orbitals leading to more conspicuous deviations in ρ. This is probably because the $np_{1/2}$ orbitals are relativistically contracted (similar to the ns orbitals), while the $np_{3/2}$ orbitals resemble nonrelativistic np orbitals. Therefore, the DF calculations that neglect core-valence correlation (see column 1 of Table II) cannot adequately represent either the observed absolute values of oscillator strength or their ratios. The inclusion of the core-valence correlation in

TABLE II. Comparison of calculated and experimental f values and the fine-structure component ratios ρ in the principal series of Rb. The column headings DF, DF+CPI, and DF+CPII are explained in Sec. III A. Numbers in square brackets represent powers of ten.

	Theory				Experiment		
n	DF	DF+CPI	DF+CPII	Hofsaess [34]	Caliebe and Niemax [30]	Shabanova and Khlyustalov [31]	Goltz *et al*. [32]
					$f(5s_{1/2}\rightarrow np_{1/2})$		
5	3.74[−1]	3.43[−1]	3.45[−1]	3.36[−1]		3.32[−1]	
6	5.10[−3]	3.53[−3]	3.65[−3]	3.53[−3]	4.0±0.4[−3]	3.73[−3]	
7	8.70[−4]	4.50[−4]	4.80[−4]	4.04[−4]	5.6±0.5[−4]	4.87[−4]	
8	2.94[−4]	1.21[−4]	1.32[−4]	1.16[−4]	1.5±0.2[−4]	1.38[−4]	
9	1.36[−4]	4.68[−5]	5.25[−5]	4.36[−5]	6.0±0.7[−5]	5.22[−5]	
10	7.45[−5]	2.26[−5]	2.58[−5]	2.05[−5]	3.0±0.3[−5]	2.61[−5]	
11	4.57[−5]	1.26[−5]	1.46[−5]	1.12[−5]	1.85±0.2[−5]	1.46[−5]	
12	3.02[−5]	7.71[−6]	9.04[−6]	6.77[−6]	9.95±0.9[−6]	9.00[−6]	
13	2.11[−5]	5.08[−6]	6.02[−6]	4.43[−6]	6.05[−6] [a]	5.82[−6]	
14	1.54[−5]	3.54[−6]	4.22[−6]	2.94[−6]	4.59[−6]	3.97[−6]	
15	1.16[−5]	2.57[−6]	3.08[−6]	2.07[−6]	2.69[−6]	2.74[−6]	
16	8.96[−6]	1.93[−6]	2.32[−6]	1.49[−6]	2.27[−6]		
17	7.08[−6]	1.49[−6]	1.80[−6]	1.09[−6]	1.75[−6]		
18	5.70[−6]	1.17[−6]	1.42[−6]	8.53[−7]	1.43[−6]		
19	4.65[−6]	9.41[−7]	1.15[−6]	6.58[−7]			
20	3.85[−6]	7.68[−7]	9.39[−7]	4.93[−7]			
21	3.23[−6]	6.36[−7]	7.79[−7]				
22	2.73[−6]	5.33[−7]	6.53[−7]				
23	2.33[−6]	4.51[−7]	5.54[−7]				
24	2.01[−6]	3.85[−7]	4.74[−7]				
25	1.74[−6]	3.33[−7]	4.10[−7]				
					$f(5s_{1/2}\rightarrow np_{3/2})$		
5	7.58[−1]	6.97[−1]	7.03[−1]	6.28[−1]		6.68[−1]	
6	1.27[−2]	9.25[−3]	9.76[−3]	9.47[−3]	9.37±0.7[−3]	9.54[−3]	
7	2.38[−3]	1.41[−3]	1.55[−3]	1.44[−3]	1.53±0.1[−3]	1.48[−3]	
8	8.54[−4]	4.31[−4]	4.90[−4]	4.38[−4]	4.60±0.4[−4]	4.68[−4]	
9	4.09[−4]	1.85[−4]	2.16[−4]	1.86[−4]	2.00±0.3[−4]	1.97[−4]	
10	2.30[−4]	9.65[−5]	1.14[−4]	9.65[−5]	1.01±0.1[−4]	1.08[−4]	
11	1.44[−4]	5.69[−5]	6.85[−5]	5.62[−5]	7.30±0.6[−5]	6.38[−5]	
12	9.61[−5]	3.66[−5]	4.44[−5]	3.60[−5]	4.25±0.3[−5]	4.09[−5]	
13	6.78[−5]	2.50[−5]	3.06[−5]	2.42[−5]	2.95±0.2[−5]	2.86[−5]	
14	4.98[−5]	1.79[−5]	2.20[−5]	1.73[−5]	2.28±0.2[−5]	2.00[−5]	
15	3.77[−5]	1.33[−5]	1.64[−5]	1.25[−5]	1.36±0.1[−5]	1.44[−5]	
16	2.92[−5]	1.02[−5]	1.26[−5]	9.55[−6]	1.13±0.1[−5]		
17	2.32[−5]	7.95[−6]	9.91[−6]	7.28[−6]	8.89±0.8[−6]		
18	1.87[−5]	6.35[−6]	7.94[−6]	5.96[−6]	7.16±0.8[−6]		
19	1.53[−5]	5.16[−6]	6.46[−6]	4.65[−6]	5.56±0.6[−6]		
20	1.27[−5]	4.25[−6]	5.33[−6]	3.67[−6]	3.84±0.4[−6]		
21	1.07[−5]	3.54[−6]	4.45[−6]				
22	9.04[−6]	2.99[−6]	3.76[−6]				
23	7.73[−6]	2.54[−6]	3.20[−6]				
24	6.67[−6]	2.19[−6]	2.75[−6]				
25	5.79[−6]	1.89[−6]	2.39[−6]				
					$\rho=f(5s_{1/2}\rightarrow np_{3/2})/f(5s_{1/2}\rightarrow np_{1/2})$		
5	2.025	2.029	2.037	2.03		2.01	
6	2.484	2.621	2.677	2.68	2.4±0.2	2.56	
7	2.742	3.124	3.226	3.27	2.6±0.2	3.04	
8	2.906	3.573	3.708	3.79	2.9±0.2	3.39	
9	3.014	3.956	4.110	4.27	3.4±0.2	3.77	3.2
10	3.089	4.273	4.437	4.70	3.6±0.1	4.14	3.5
11	3.142	4.533	4.701	5.04	4.07±0.1	4.37	3.7

TABLE II. (*Continued*)

	Theory				Experiment		
n	DF	DF+CPI	DF+CPII	Hofsaess [34]	Caliebe and Niemax [30]	Shabanova and Khlyustalov [31]	Goltz *et al.* [32]
12	3.180	4.745	4.913	5.32	4.32±0.1	4.54	4.1
13	3.209	4.918	5.084	5.58	4.88 [b]	4.91	4.4
14	3.232	5.059	5.223	5.88	4.97	5.04	4.8
15	3.249	5.176	5.336	6.04	5.06	5.26	4.7
16	3.263	5.273	5.430	6.42	4.97		4.9
17	3.275	5.354	5.509	6.70	5.09		5.4
18	3.284	5.422	5.574	6.99	5.00		
19	3.292	5.480	5.630	7.07			
20	3.298	5.530	5.677	7.45			
21	3.304	5.573	5.718				
22	3.309	5.610	5.753				
23	3.313	5.642	5.784				
24	3.316	5.670	5.810				
25	3.319	5.686	5.825				

[a]Values of $f(5s\rightarrow np_{1/2})$ oscillator strengths recalculated using the corrected oscillator strength ratios (see footnote b) and earlier $f(5s\rightarrow np_{3/2})$ values measured by Caliebe and Niemax [30].
[b]Corrected oscillator strength ratios measured recently by Niemax (see [32]).

the simplified classical core-polarization picture even with an arbitrarily chosen cutoff radius (set to the mean radius of the unpolarized ionlike core; see DF+CPI calculations of column 2 in Table II) decisively improves the agreement with experiment. Since the analysis of our results shows that the main contribution of the core polarization comes from the modification of the dipole transition operator, further refinement and improvement can be achieved if the cutoff radius in Eq. (11) can be adjusted separately for the two fine-structure components to reproduce the experimentally known position of the Cooper minimum (DF+CPII). The experimental position of the Cooper minimum as a function of the photon energy is known only for the sum of the $\epsilon p_{1/2}$ and $\epsilon p_{3/2}$ continuum channels.

It may also be noted in Table II that the model potential results of Hofsaess [34], who adjusted the cutoff radius to reproduce the experimentally determined (by Baum *et al.* [35]) Fano function $\chi(E)$ are too small for the $f(5s\rightarrow np_{1/2})$ component and hence too large for ρ of transitions to highly excited states. (The Fano function [36] $\chi(E)$ is a function of excitation energy E, directly related to ρ by the formula $\rho=2[\chi(E)+1]^2/[\chi(E)-2]^2$.)

Figure 1 presents the comparison of ρ calculated in the present work with other theoretical and experimental data. Among the experimental data, we included the result of Liberman and Pinard [37], who found that the f-value ratio for $29\leqslant n\leqslant 50$ is 5.9 ± 1.4 and, within the experimental uncertainty, does not depend on n.

As can be seen from Fig. 1, our final results (DF+CPII) agree favorably with available experimental data, whereas the Dirac-Fock data obtained without the core polarization (DF) are too low and the model-potential results of Hofsaess are definitely too high. In particular, good agreement has been found with the relative measurements of Shabanova and Khlyustalov [31] by the hook method, which produces very accurate f-value ratios.

B. Continuum dipole oscillator strengths

A prominent feature of the photoionization cross section, which is proportional to df/dw, of all alkali-metal atoms is the Cooper minimum [38], at which the cross section reaches a minimum. In the vicinity of the Cooper minimum, the dipole transition matrix element vanishes as it switches sign. The photon energy at which the matrix element vanishes is

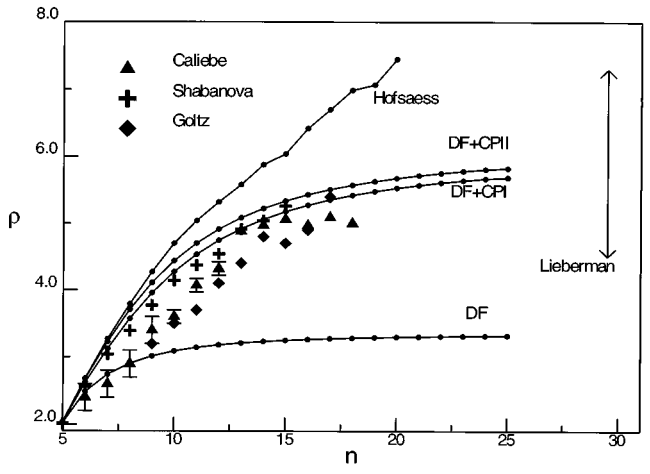

FIG. 1. Ratio ρ of f values (see Table II) vs principal quantum number of the upper state for the principal series of Rb. DF, present work with no CPP; DF+CPI, present work with the same cutoff radii for the potential and the dipole operator; DF+CPII, present work with cutoff radii in the dipole operator adjusted to reproduce the Cooper minimum; Hofsaess, model potential result by Hofsaess [34]; triangles, experimental data by Caliebe and Niemax [30]; crosses, data by Shabanova and Khlyustalov [31]; diamonds, data by Goltz *et al.* [32]; Liberman, high-n ratios measured by Liberman and Pinard [37].

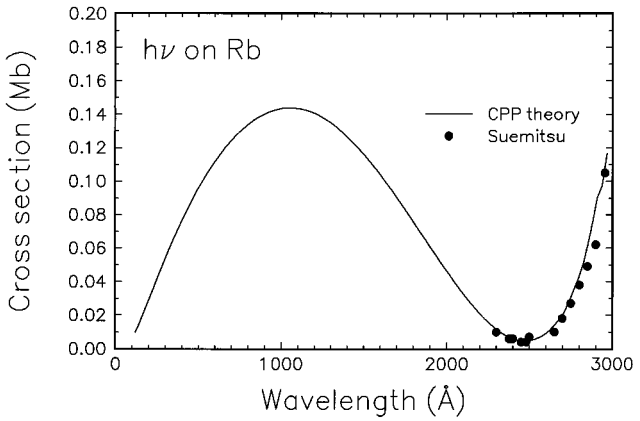

FIG. 2. Comparison of photoionization cross sections. Solid curve, present work; circles, experiment by Suemitsu and Samson [19].

slightly different for the $5s \rightarrow \epsilon p_{1/2}$ and the $5s \rightarrow \epsilon p_{3/2}$ transitions, which is why the observed cross section at the minimum does not vanish.

The departure of the ratio ρ from the statistical ratio of 2 is a clear indication that the minima for the two continuum channels occur at different photon energies. When df/dw for the $5s \rightarrow \epsilon p_{1/2}$ transition vanishes, $\rho \rightarrow \infty$ unless df/dw for the $5s \rightarrow \epsilon p_{3/2}$ transition also vanishes at the same photon energy. There have been many *ab initio* calculations to reproduce the position and the shape of df/dw near the Cooper minimum, but they had only limited success.

As mentioned earlier, we adjusted the cutoff radii in our CPP model so that we could generate a consistent set of f values for the principal series and df/dw that reproduced not only the observed shape and position of the Cooper minimum when the $\epsilon p_{1/2}$ and $\epsilon p_{3/2}$ results were combined but also the df/dw for each channel connected smoothly with the matching discrete f values at the ionization threshold as required by the quantum-defect theory.

The photoionization cross section calculated in this way is compared with the experimental data by Suemitsu and Samson [19] in Fig. 2. The experiment is a relative measurement with an error limit of $\pm 2\%$ for its shape and its magnitude was normalized to a CPP model calculation by Weisheit [1].

For our purpose, it is convenient to have df/dw in an analytic form so that we can integrate it to an arbitrary value of w [see Eq. (6)]. Since the transition matrix element, but not df/dw, varies smoothly across the Cooper minimum, we fitted the square root of df/dw to an inverse power series of w:

$$\sqrt{\frac{df}{dw}} = \frac{a_1}{w} + \frac{a_2}{w^2} + \frac{a_3}{w^3} + \frac{a_4}{w^4} + \frac{a_5}{w^5} + \frac{a_6}{w^6}, \qquad (12)$$

where the values of the fitting coefficients a_i are listed in Table III. By definition, the value of w runs from 1 to ∞. In Table IV we present the sum of f values for discrete excitations, N_i defined in Eq. (7) for the $\epsilon p_{1/2}$ and $\epsilon p_{3/2}$ channels, and their ratios.

TABLE IV. Sum of discrete f values and N_i [see Eq. (7)], and their ratios.

Transition	Sum of discrete f_n	N_i
$5s \rightarrow np_{1/2}$, $\epsilon p_{1/2}$	0.349 ($n \leqslant 25$)	0.0184
$5s \rightarrow np_{3/2}$, $\epsilon p_{3/2}$	0.715 ($n \leqslant 25$)	0.0255
Ratio ($p_{3/2}/p_{1/2}$)	2.05	1.38

IV. ELECTRON-IMPACT IONIZATION CROSS SECTION

With the df/dw for the $5s \rightarrow \epsilon p$ transition in an analytic form, we can now easily calculate the cross section for the ionization of the $5s$ electron σ_{5s} using Eq. (5). However, we must also include ionization cross sections of the core electrons, in which the core electrons are ejected directly into the continuum, to obtain the total ionization cross section σ_{ion}. We used the BEB cross section [Eq. (9)] to calculate the direct ionization contribution of the core electrons. In addition, the core electrons can be excited to discrete levels ns, $np, nd, \ldots, n \geqslant 5$, and then autoionize, thus eventually contributing to the total ionization cross section. These indirect ionization processes are numerous, though individual cross sections are very small compared to σ_{5s}. As explained below, the sum of these autoionizing excitation cross sections of the $4s$ and $4p$ electrons exceeds the sum of direct ionization of the core electrons. This large contribution from the autoionizing excitations of the loosely bound core orbitals is a typical feature of alkali-metal atoms and alkali-metal-like ions.

A. Direct ionization cross section

The cross sections for the direct ionization of the core electrons have been calculated using the BEB model [Eq. (9)], which does not require the detailed knowledge of individual df/dw. The orbital constants needed to calculate BEB cross sections are given in Table I. Orbital constants for the K and L shells are omitted because they do not contribute much to σ_{ion} unless the incident energy is extremely high. The sum of the BEB cross sections for the direct ionization of the core electrons σ_{core} is compared to σ_{5s} in Fig. 3; σ_{core} amounts to about one-half of σ_{5s} at $T = 100$ eV.

B. Autoionizing excitations of 4s and 4p electrons

Electron-impact cross sections for the excitation of the $4s$ and $4p$ electrons to many levels arising from the $4s4p^6 5s^2$, $4s4p^6 5s5p$, $4s^2 4p^5 5s^2$, $4s^2 4p^5 5s5p$, and $4s^2 4p^5 5s4d$

TABLE III. Fitting coefficients for $\sqrt{df/dw}$ [see Eq. (12)].

Orbital	a_1	a_2	a_3	a_4	a_5	a_6
$\epsilon p_{1/2}$	1.4406	−8.0075	21.064	−29.649	21.128	−6.0005
$\epsilon p_{3/2}$	−1.7196	9.4637	−24.413	33.896	−23.902	6.7372

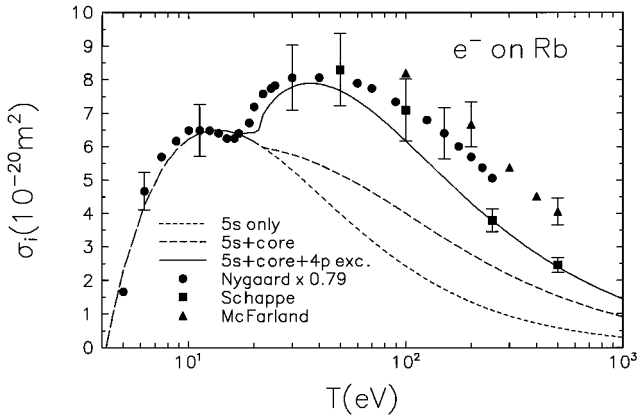

FIG. 3. Comparison of electron-impact ionization cross sections. Solid curve, present theory for the total ionization cross section; short-dashed curve, present theory for the ionization of the $5s$ electron only; medium-dashed curve, present theory for the direct ionization; circles, gross ionization cross section measured by Nygaard and Hahn [10] (reduced by a factor of 0.79); squares, counting ionization cross section measured by Schappe *et al.* [14]; triangles, gross ionization cross section measured by McFarland and Kinney [9] as quoted by Kieffer and Dunn [39].

configurations were calculated using the plane-wave Born approximation. The radial wave functions were generated using the $(2J+1)$-weighted configuration average of Dirac-Fock wave functions and then the radial functions were frozen to generate appropriate eigenfunctions of J^2.

Among these autoionizing excitations, the cross sections for the excitations of the $4s$ electron contribute only about 1% of the sum of the autoionizing excitations. For the excitation of the $4p$ electrons, we included excitations to two levels $^2P_{1/2}$ and $^2P_{3/2}$ from the $4p^5 5s^2$ configuration; four $J=1/2$ levels, seven $J=3/2$ levels, seven $J=5/2$ levels, and four $J=7/2$ levels from the $4p^5 5s 4d$ configuration; and six $J=1/2$ levels and seven $J=3/2$ levels from the $4p^5 5s 5p$ configuration. Of the excitations to these 37 levels, only three dipole-allowed transitions had peak values exceeding 10^{-21} m^2, viz., excitations to the $4s^2 4p^5 5s^2\ ^2P_{3/2}$, $4s^2 4p^5 5s 4d\ ^2P_{1/2}$, and $^2P_{3/2}$ levels. As expected, the dipole-allowed transitions peak at $T\sim 55$ eV, while the rest peak at $T\sim 30$ eV.

The dipole-allowed excitation cross sections account for almost 90% of the sum. Since Born cross sections tend to be too high near the peak, we expect that the sum of the Born cross sections presented in Fig. 3 may be an overestimate. However, there are many more weak transitions we have omitted, raising the possibility that the overestimate by the Born approximation may be canceled to some extent by the autoionizing excitation cross sections we have omitted.

C. Comparison with experiment

The theoretical and experimental data presented in Fig. 3 clearly indicate that the combination of the BED, BEB, and Born cross sections reproduces the shape of the experimental cross sections very well. The data by Nygaard and Hahn [10] in Fig. 3 were reduced by 21% to demonstrate the agreement in shape with the shape of the theory. The lowest energy needed to produce a doubly charged ion is $\sim$31.5 eV. Some of the difference between theory and experiments at $T>30$ eV could have come from the fact that the experiments, except for that by Schappe *et al.* [14], measured gross ionization cross sections.

TABLE V. Theoretical partial and total ionization cross sections (in 10^{-20} m^2).

T (eV)	σ_{BED}, $5s$ only	σ_{BEB}, core	Born, $4s+4p$	Total
5	2.31			2.31
10	6.23			6.23
15	6.47			6.47
20	6.15		0.28	6.43
30	5.30	0.47	2.02	7.79
40	4.58	0.89	2.41	7.88
50	4.00	1.17	2.50	7.68
70	3.19	1.46	2.41	7.06
100	2.43	1.58	2.16	6.17
200	1.36	1.42	1.53	4.31
300	0.94	1.22	1.22	3.39
400	0.72	1.07	1.01	2.80
500	0.59	0.95	0.87	2.40
750	0.40	0.75	0.66	1.80
1000	0.30	0.62	0.53	1.45

McFarland and Kinney [9] reported that the gross ionization cross section for the production of Rb^{2+} at $T=100$ eV was one-half of the cross section for Rb^+, or approximately 2×10^{-20} m^2. To convert this to the counting ionization cross section, we divide the gross ionization cross section by 2. This makes the difference between the counting and gross ionization cross section for Rb^{2+} at $T=100$ eV approximately 1×10^{-20} m^2. This is actually the size of the difference between the experiment by Schappe *et al.* [14] and McFarland and Kinney. The difference between the theory and the data by McFarland and Kinney is much larger and cannot be easily accounted for by using the cross sections for multiple ionizations reported by them.

The theory used the plane-wave Born approximation for the autoionizing excitations and hence it is likely to be an overestimate rather than an underestimate at $T>20$ eV. The theory includes direct ionization of inner-shell electrons, which can in turn lead to further stages of ionization through a series of Auger transitions to fill the inner-shell hole. A hole in the $4p$ subshell cannot lead to an Auger process because there is only one valence electron. Although a hole in the $4s$ subshell or deeper can lead to an Auger process, the combined cross section for creating a deep inner-shell hole is, according to our calculation, less than 0.2×10^{-20} m^2, mostly from the $4s$ subshell. Hence the difference between the theory and some experiments presented in Fig. 3 at $T>100$ eV is unlikely to have resulted from multiple ionization alone. Our theoretical total and partial cross sections for electron-impact ionization are presented in Table V.

V. CONCLUSIONS

Comparisons to experiments presented in Figs. 1 and 3 clearly indicate that (a) the core-polarization potential method can be used to simulate core-valence correlation ef-

fectively and (b) the binary-encounter dipole model in combination with the Born approximation can explain the shape and magnitude of the ionization cross section of Rb by electron impact. The double-peak feature of the Rb cross section should also appear in other alkali-metal atoms for the same reason: The first peak comes from the direct ionization of the valence electron, while the second peak is the sum of a large number of autoionizing excitations of the loosely bound core electrons. As can be seen from Fig. 3, the autoionizing excitations contribute about one-third of the total ionization cross section for $T>25$ eV.

The oscillator-strength sums presented in Table IV demonstrate the dominance of the discrete spectrum. Since N_i is very small compared to unity, or the number of valence electrons, one could have obtained a quick estimate of σ_{5s} by setting $D(t)=N_i=0$ in Eq. (5) without calculating df/dw. This would have led to σ_{5s} slightly higher than that shown in Fig. 3. Work is in progress to calculate similar ionization cross sections for other alkali-metal atoms.

ACKNOWLEDGMENTS

This work was supported in part by a grant from the U.S.-Poland Maria-Skłodowska-Curie Joint Fund II and the work at NIST was also partly supported by the Office of Fusion Energy of the U.S. Department of Energy. We are greatly indebted to J. P. Desclaux for his Dirac-Fock wave function code, which we modified to include the core-polarization potential to calculate f values and df/dE. We also thank C. C. Lin for providing us with the numerical values of the experimental data in Ref. [14] and J. Berkowitz and J. A. R. Samson for discussions on photoionization cross-section measurements. J. B. thanks NIST for its hospitality during his year-long stay there when this work was performed.

[1] J. C. Weisheit, Phys. Rev. A **5**, 1621 (1972).
[2] D. W. Norcross, Phys. Rev. A **7**, 606 (1973).
[3] J. Migdałek and W. E. Baylis, J. Quant. Spectrosc. Radiat. Transf. **22**, 127 (1979).
[4] J. Migdałek and W. E. Baylis, Can. J. Phys. **57**, 1708 (1979).
[5] F. Rasetti, Nuovo Cimento **1**, 115 (1924).
[6] E. Fermi, Z. Phys. **59**, 680 (1930).
[7] J. T. Tate and P. T. Smith, Phys. Rev. **46**, 773 (1934).
[8] G. O. Brink, Phys. Rev. **134**, A345 (1964).
[9] R. H. McFarland and J. D. Kinney, Phys. Rev. **137**, A1058 (1965).
[10] K. J. Nygaard and Y. B. Hahn, J. Chem. Phys. **58**, 349 (1973).
[11] M. Gryzinski, Phys. Rev. **138**, A305 (1965); **138**, A322 (1965); **138**, A336 (1965).
[12] R. H. McFarland, Phys. Rev. **139**, A40 (1965).
[13] W. Lotz, Astrophys. J. **14**, 207 (1967).
[14] R. S. Schappe, T. Walker, L. W. Anderson, and C. C. Lin, Phys. Rev. Lett. **76**, 4328 (1996).
[15] Y.-K. Kim and M. E. Rudd, Phys. Rev. A **50**, 3954 (1994).
[16] W. Hwang, Y.-K. Kim, and M. E. Rudd, J. Chem. Phys. **104**, 2956 (1996).
[17] Y.-K. Kim, W. Hwang, N. M. Weinberger, M. A. Ali, and M. E. Rudd, J. Chem. Phys. **106**, 1026 (1997).
[18] M. A. Ali, Y.-K. Kim, W. Hwang, N. M. Weinberger, and M. E. Rudd, J. Chem. Phys. **106**, 9602 (1997).
[19] H. Suemitsu and J. A. R. Samson, Phys. Rev. A **28**, 2752 (1983).
[20] Y.-K. Kim and J. P. Desclaux, Phys. Scr. **36**, 796 (1987).
[21] N. F. Mott, Proc. R. Soc. London, Ser. A **126**, 259 (1930).
[22] L. Vriens, in *Case Studies in Atomic Physics*, edited by E. W. McDaniel and M. R. C. McDowell (North-Holland, Amsterdam, 1969), Vol. 1, p. 335.
[23] H. Bethe, Ann. Phys. (Leipzig) **5**, 325 (1930).
[24] M. Inokuti, Rev. Mod. Phys. **43**, 297 (1971).
[25] L. Biermann, Z. Astrophys. **22**, 157 (1943).
[26] W. Heisenberg, Z. Phys. **39**, 499 (1926).
[27] C. Böttcher and A. Dalgarno, Proc. R. Soc. London, Ser. A **340**, 187 (1974).
[28] J. Migdałek and W. E. Baylis, J. Phys. B **11**, L497 (1978).
[29] W. R. Johnson, D. Kolb, and K.-N. Huang, At. Data Nucl. Data Tables **28**, 333 (1983).
[30] E. Caliebe and K. Niemax, J. Phys. B **12**, L45 (1979).
[31] L. N. Shabanova and A. N. Khlyustalov, Opt. Spektrosk. **56**, 205 (1984) [Opt. Spectrosc. **56**, 128 (1984)].
[32] D. Goltz, W. Hansen, and J. Richter, Phys. Scr. **30**, 244 (1984).
[33] J. Migdałek, Acta Phys. Pol. A **54**, 253 (1978).
[34] D. Hofsaess, Z. Phys. A **281**, 1 (1977).
[35] G. Baum, M. S. Lubell, and W. Raith, Phys. Rev. Lett. **25**, 267 (1970).
[36] U. Fano, Phys. Rev. **178**, 131 (1969).
[37] S. Liberman and J. Pinard, Phys. Rev. A **20**, 507 (1979).
[38] G. V. Marr and D. M. Creek, Proc. R. Soc. London, Ser. A **304**, 233 (1968); **304**, 245 (1968).
[39] L. J. Kieffer and G. H. Dunn, Rev. Mod. Phys. **38**, 1 (1966).